Molecular Reaction Mechanisms of Proteins Monitored by Nanosecond Step-Scan FT-IR Difference Spectroscopy

ROBIN RAMMELSBERG, BENEDIKT HEßLING, HARALD CHORONGIEWSKI, and KLAUS GERWERT*

Ruhr-Universität Bochum, Lehrstuhl für Biophysik, D-44780 Bochum, Germany

Step-scan FT-IR difference spectroscopy with 100-ns time resolution is applied to the membrane protein bacteriorhodopsin. The experimetal setup and data acquisition are described in great detail. The IR absorbance changes accompanying bacteriorhodopsin's photocycle are presented in a three-dimensional representation. The data quality allows one, for example, to resolve the biphasic rise of the photocycle-intermediate M. A bacteriorhodopsin's proton pump model based on the FT-IR works is presented.

Index Headings: **Step-scan FT-IR; Proton pump mechanism; Bacteriorhodopsin; Time-resolved FT-IR; Molecular reaction mechanism.**

INTRODUCTION

Time-resolved FT-IR difference spectroscopy has recently been established as a new biophysical tool for the investigation of molecular reaction mechanisms of proteins at the atomic level.[1] Complementary to NMR spectroscopy and X-ray structure analysis, which provide the static protein ground-state structure with atomic resolution, time-resolved FT-IR difference spectroscopy monitors the dynamics of proteins at the atomic level. Performing difference spectroscopy between the protein ground state and activated states selects only the absorbance changes of the protein groups involved in the function. This approach eliminates the large background absorbance of the quiescent parts of the protein, the water, and the buffer.

In protein chemistry the macromolecule studied most intensely thus far by time-resolved FT-IR difference spectroscopy is the light-driven proton pump bacteriorhodopsin. Many research groups worldwide have contributed to the understanding of the mechanism of this membrane protein.[2] For reviews on FT-IR work on bacteriorhodopsin, see Refs. 3, 4, and 5. Time-resolved FT-IR spectroscopy has furthermore provided a detailed picture of the light-induced electron transfer mechanisms of bacterial photosynthetic reaction centers.[6] For reviews and recent FT-IR work, see Refs. 7, 8, and 9. Besides photobiological proteins, time-resolved FT-IR spectroscopy can also be applied to proteins without an intrinsic chromophore by using photolabile trigger compounds.[10] With the use of "caged" GTP, the molecular GTPase mechanism of the oncogenic protein H-ras p21, a molecule that plays a central role in the growth of cancer cells,[11] can be monitored.[12] Another example is "caged" Ca^{2+}, by which one can investigate the molecular mechanism of the Ca^{2+}-ATPase.[13,14] Furthermore "caged" electrons can be used to study redox reactions in proteins.[15]

Various time-resolved FT-IR techniques exist: the rapid-scan technique, which gives millisecond time resolution,[16–18] the stroboscope technique, which gives microsecond time resolution,[19,20] and the step-scan technique.[21,22] Here we focus on our group's time-resolved, step-scan FT-IR studies of bacteriorhodopsin, now yielding 100-ns time resolution. The excellent signal-to-noise ratio allows, for the first time, the resolution of the biphasic rise of bacteriorhodopsin's M intermediate in the infrared spectral region. The step-scan technique will be used in the future to investigate fast reactions of the other proteins mentioned.

MATERIALS AND METHODS

Our experimental setup is shown in Fig. 1. The FT-IR apparatus, with globar, beamsplitter, fixed and movable mirrors, and photovoltaic detector, is based on a Bruker IFS66v spectrometer.

Laser Excitation. Excitation of the sample is achieved by a dye laser (Lambda Physik, FL105, emission at 546 nm, 3 mJ at the sample). The dye laser is pumped by a XeCl excimer laser system (Lambda Physik, LPX240i). Pulse duration is about 20 ns. The interference filter in the laser beam is used to narrow the laser emission to 546±2.5 nm.

Visible Spectroscopy. Simultaneously to IR measurements, absorbance changes in the visible spectral range are also monitored by a conventional photolysis setup. The measuring light of a 100-W halogen lamp passes through an interference filter before illuminating the sample. Between the sample and the photomultiplier (rise time 20 ns) a monochromator and a second interference filter are positioned to eliminate the actinic radiation of the dye laser.

Step-Scan Spectroscopy. Except for the home-built sample chamber, the FT-IR apparatus is evacuated to 3 mbar during measurement. This condition increases the stability and reduces the sound sensitivity of the movable mirror. Furthermore, the setup is positioned on a vibration isolation table (Newport) in a temperature-controlled laboratory. We have determined the residual fluctuations of the movable mirror to be ± 0.5 nm. The sample chamber is purged with dry air (dew point −70 °C, Balston 75-62 FT-IR purge gas generator). The IR absorbance changes are detected by a photovoltaic HgMnTe detector (Kollmar Tech., KV100-1-B-7/190, cutoff 850 cm^{-1}). The detector's signal is amplified in a home-built two-stage preamplifier with an ac- and a dc-coupled output. The bandwidth of the dc part is limited to 200 kHz, whereas the

Received 31 July 1996; accepted 3 December 1996.

* Author to whom correspondence should be sent.

0003-7028/97/5104-0558$2.00/0

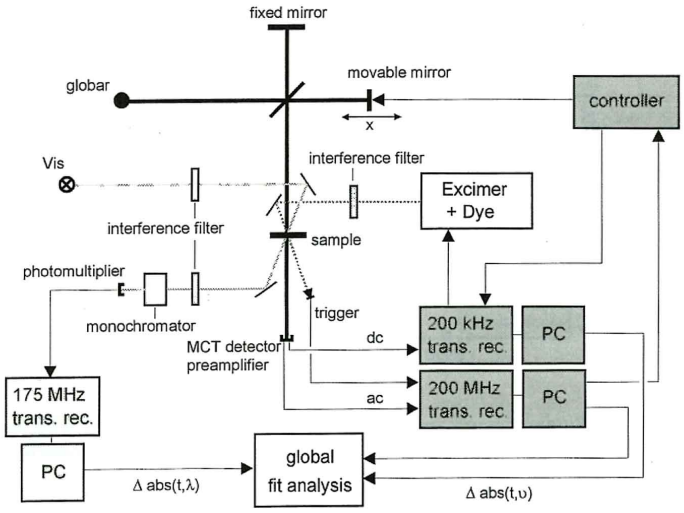

FIG. 1. The experimental setup, consisting of an FT-IR apparatus (Bruker IFS66v) with globar, beamsplitter, mirrors, controller, detector, and preamplifier connected to a 200-kHz and a 200-MHz transient recorder; a photolysis setup with light source, interference filters, monochromator, photomultiplier, and transient recorder; and an excimer pumped dye laser system to activate the sample. The visible and IR data are transferred to a workstation (SUN) network for kinetic analysis.

bandwidth of the ac part is 10 MHz. Controls ensure that the output signal of the preamplifier depends linearly on the IR intensity.

The dc-coupled output of the preamplifier is digitized by a 12-bit, 200-kHz transient recorder (Keithley, ADWIN 8) connected to a PC. The offset of the input signal can be compensated to zero. This capability allows subsequent amplification of the signal and allows use of the full dynamic range of the transient recorder. The bacteriorhodopsin photocycle comprises reactions from the nanosecond to the millisecond time domain. In order to prune the huge amount of data accumulated in a complete photocycle, the 200-kHz acquisition rate is slowed down to 50 kHz at 200 μs, which allows time averaging. The ac-coupled output of the preamplifier is recorded by a 200-MHz, 8-bit transient recorder (Spectrum, PAD 82).

At every sampling point of the interferogram, the correct positioning of the movable mirror is checked before data acquisition starts. A TTL output signal then triggers the excimer laser to initiate the reaction. A fast photodiode (rise time 10 ns) is activated by a reflex of the dye laser and starts data acquisition of the 200-MHz transient recorder.

The spectral range is limited below the Nyquist wavenumber 1975 cm^{-1} by an interference filter to reduce the number of sampling points of the interferogram. This filter also shields the IR detector from scattered light of the dye laser and the heat emitted by the sample. (The dye laser's pulse causes a small warming of the sample.) The resulting interferogram contains 780 points. It is multiplied with the Norton–Beer weak apodization function and then zero-filled by a factor of 2. The phase-spectrum $\phi(\nu)$ is calculated with a spectral resolution of 50 cm^{-1}, whereas the difference spectra are taken with a spectral resolution of approximately 3 cm^{-1}.

Time-resolved measurements proceed as follows (Fig. 2):

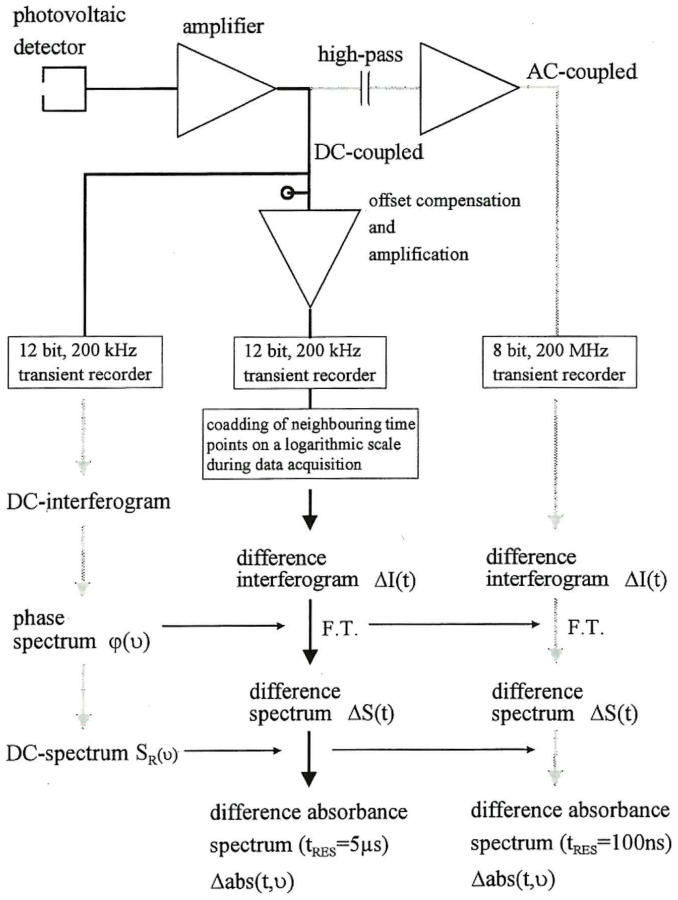

FIG. 2. A schematic representation of the IR signal preamplification, the data recording, and the calculation of the difference spectra in the dc- and ac-coupled mode.

1. A dc-interferogram is measured with the 200-kHz transient recorder in the step-scan mode without sample excitation. Thereby, no offset adjustment or further amplification of the signal is performed. This interferogram is used to calculate the phase $\phi(\nu)$ and the single-channel dc-spectrum $S_R(\nu)$.
2. The time-resolved measurement starts by a laser flash. Both transient recorders simultaneously measure the time-dependent infrared intensity changes at the respective sampling positions. The 200-MHz transient recorder measures the time domain from 100 ns to 20 μs, whereas the 200-kHz transient recorder monitors from 5 μs until the end of the reaction in the millisecond time range. At every sampling position of the interferogram, several photocycles are averaged to improve the signal-to-noise ratio. In the data shown below, 100 photocycles are accumulated. After measurement of the time courses of all interferogram sampling positions the data are rearranged to yield time-dependent difference interferograms $\Delta I(t)$ (Fig. 3). Because these difference interferograms contain positive as well as negative spectral features, the usual Mertz phase correction cannot be directly applied. Therefore, the stored phase $\phi(\nu)$ from the first measurement (step 1) is used. The phase does not change between both measurements, because the movable mirror stops at

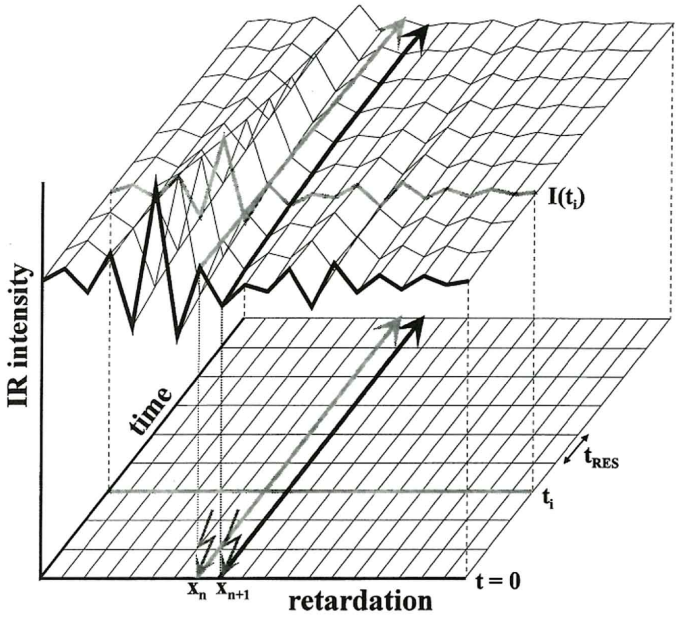

FIG. 3. Step-scan principle: In the step-scan mode the mirror is stopped at the sampling positions x_n. Then the reaction is initiated and the time dependence of the IR intensity is measured. The time resolution is restricted by the photovoltaic detector. After relaxation of the system, the scanner steps to the next position x_{n+1}, and the reaction is again started. After measuring the time dependence of all sampling positions, the computer rearranges the data to yield the time-dependent interferograms $I(t_i)$. Fourier transformation yields the time-dependent spectra.

exactly the same sampling points and only small absorbance changes take place.

Sample Preparation. Bacteriorhodopsin is purified from *Halobacterium salinarium* as purple membrane sheets by a now standard method.[23] Bacteriorhodopsin is suspended (200 μg in 2 M KCl and 0.1 M buffer) and then centrifuged to concentrate the sample into a pellet. The pellet is squeezed between two CaF_2 windows separated by a 2.5-μm spacer to depress the water background absorbance.

Global-Fit Analysis. The absorbance change ΔA in the IR at the wavenumbers ν_i are analyzed with sums of n_r exponentials with apparent rate constants k_n and amplitudes a_n, where $\{k_n\}$ is the same for all i.

$$\Delta A(\nu_i, t) = \sum_{n=1}^{n_r} a_n(\nu_i) e^{-k_n t}$$

For a detailed description, see Ref. 24.

RESULTS AND DISCUSSION

A single-channel spectrum of bacteriorhodopsin is shown in Fig. 4. Besides the sample absorbance, it reflects the instrument's spectroscopic properties. The single-channel spectrum is dominated by the strong amide I and amide II protein peptide backbone vibrations at 1650 and 1550 cm^{-1} and the O–H water bending vibration at 1650 cm^{-1}. The intensity above 1975 cm^{-1} is suppressed by an interference filter. Below 850 cm^{-1} the detector is not sensitive, and the CaF_2 windows used are not transparent below 900 cm^{-1}. The photovoltaic HgMnTe detector, which is used for the step-scan measurements, does not monitor intensity below 900 cm^{-1}. In contrast,

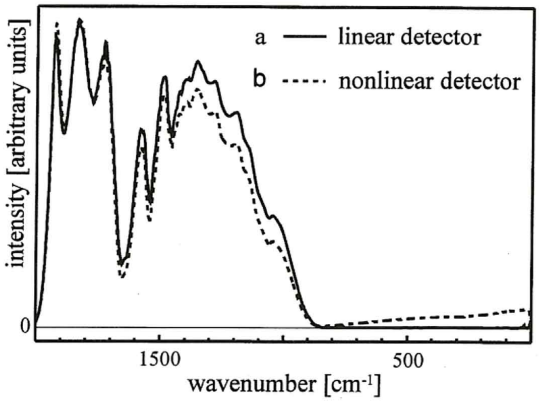

FIG. 4. Single-channel spectra of bacteriorhodopsin measured with (*a*) the photovoltaic HgMnTe detector (linear) and (*b*) a photoconductive HgCdTe detector (nonlinear).

with a "conventional" MCT photoconductive detector (Graseby D313 with Bruker preamplifier) an artifactually increasing intensity below 900 cm^{-1} (Fig. 4) appears. This artifact is caused by a nonlinear response of the detector preamplifier system. Because of this nonlinearity, the intensity of the interferogram's center peak is not reproduced correctly. Since the center peak is the most prominent peak, the nonlinearity affects only this part of the interferogram. The nonlinearity causes a decrease in the integral intensity of the single-channel spectrum. If the integral intensity changes during the reaction, the nonlinear response of the detector leads to very small broad absorbance changes in the difference spectra. These changes are significant only for very small absorbance changes. For example, the very small continuum absorbance change ($\Delta A = 3 \cdot 10^{-4}$) indicative of hydrogen-bonded networks[25] basically shows a shift of the baseline. This effect is illustrated in Fig. 5.

After light excitation, bacteriorhodopsin undergoes a photocycle, completed within 10 ms, with the intermediates K, L, M, N, and O. The photocycle is accompanied by a vectorial proton transfer through the protein. Unfortunately, laser excitation of bacteriorhodopsin induces not only the IR intensity changes accompanying the photocyle but other undesired changes in the interferogram as well. All light-induced changes of the interferogram at one sampling position are presented in Fig. 6. Fortunate-

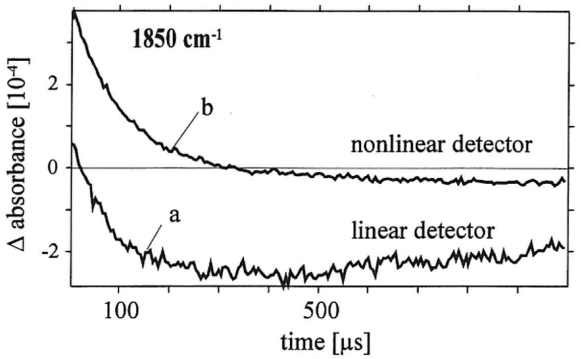

FIG. 5. Time course of a small, broad absorbance change, the continuum absorbance at 1850 cm^{-1} , measured with (*a*) the photovoltaic HgMnTe detector (linear) and (*b*) the nonlinear photoconductive HgCdTe detector (nonlinear). This nonlinearity mostly leads to a baseline shift.

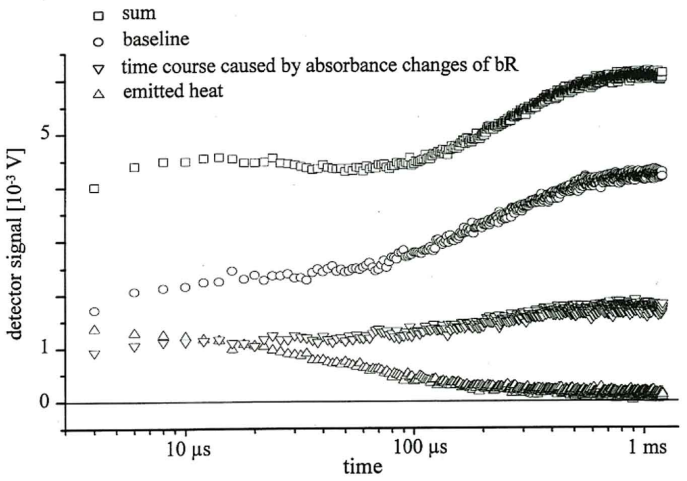

FIG. 6. The light-induced IR-changes at a single sampling position. Besides the IR changes caused by the photocycle of bacteriorhodopsin (▽), changes due to the heat radiation caused by the warming of the sample by the dye laser pulse (△) are seen. The heat radiation is measured with a blocked IR source. It disappears with a 50-µs half-life. Because the radiation is not modulated by the Michelson interferometer, it is not spectrally resolved. In addition the baseline (○) shows further shifts because the whole background absorbance of the sample changes for the photocycle intermediates as compared to the ground state. To obtain the baseline shift, we measure and average the intensity changes far away from the center peak at different sampling positions. Afterwards, the heat radiation, which also contributes, is subtracted from the time course. The baseline shift contributes only to the offset of the interferograms, because it is the same at every sampling position. Fortunately, these undesired changes do not contribute to the absorbance difference spectra.

ly, the baseline shift and the heat emission of the sample show the same time course for every sampling position of the interferogram. Therefore they do not contribute to the difference spectra. In Fig. 7 the IR absorbance changes between 1800 and 1000 cm^{-1} during the photocycle are shown in a three-dimensional representation. Beyond a background absorbance of up to one absorbance unit, changes on the order of 10^{-3} to 10^{-4} are monitored with 3 cm^{-1} spectral resolution and 100-ns time resolution. As an example, the absorbance change at 1188

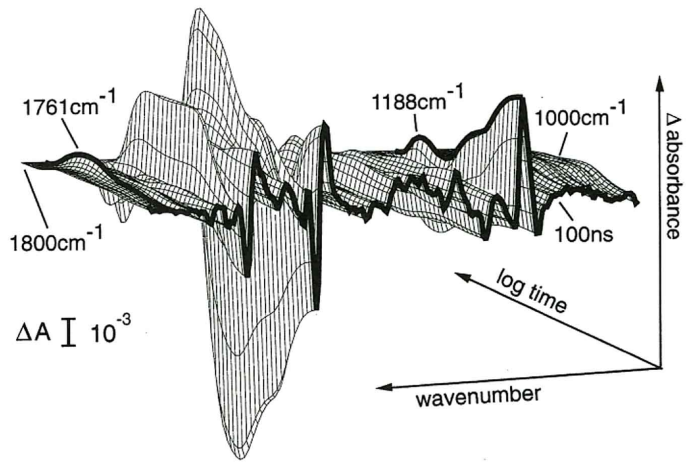

FIG. 7. A three-dimensional representation of the IR absorbance changes between 1800 and 1000 cm^{-1} with 100-ns time resolution and 3-cm^{-1} spectral resolution accompanying bacteriorhodopsin's photocycle as revealed by a global-fit analysis. The time axis has a logarithmic scale in order to show a complete bacteriorhodopsin photocycle in one representation.

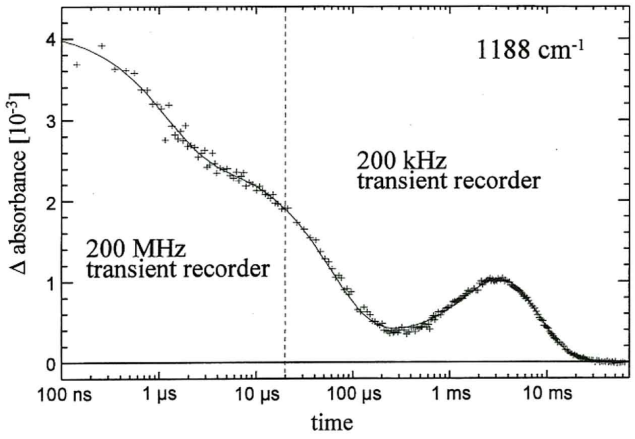

FIG. 8. An example of a time course. The absorbance changes at 1188 cm^{-1} from Fig. 7 is shown. Because the data are recorded simultaneously with the 200-kHz and the 200-MHz transient recorder, no inconsistency is seen in the overlap region near 20 µs. The band represents a C–C stretching vibration of 13-*cis* protonated Schiff base retinal.

cm^{-1} is presented as a function of time in Fig. 8. The appearance of this C–C stretching vibration band at 100 ns indicates the all-*trans* to 13-*cis* isomerization of retinal, which takes place within 450 fs (see also Fig. 10). Its disappearance at about 200 µs indicates the deprotonation of the Schiff base. This loss of charge greatly reduces the IR absorbance of the chromophore. [The Schiff base connects the retinal to Lys216 of the protein (Fig. 10).] The deprotonation kinetics of the Schiff base agree nicely with the protonation kinetics of the counterion Asp85, which can be followed at 1761 cm^{-1} (Fig. 7).[26,27,28] The reappearance of the peak at 1188 cm^{-1} in the millisecond time domain indicates the reprotonation of the Schiff base by Asp96[18,28] (Fig. 10). Its final disappearance shows the protein's relaxation to the BR-ground state.

As a demonstration of the high data quality, we now resolve the biphasic M rise in the infrared. In Fig. 9 the amplitude spectra of the two rate constants k_2 and k_5 from the global-fit analysis, which describe the biphasic M rise, are shown. With the stroboscope technique, the biphasic rise of M could not be resolved in the IR.[19,20,24] Now, for the first time, one can show that the k_2 amplitude spectrum represents bacteriorhodopsin's intramolec-

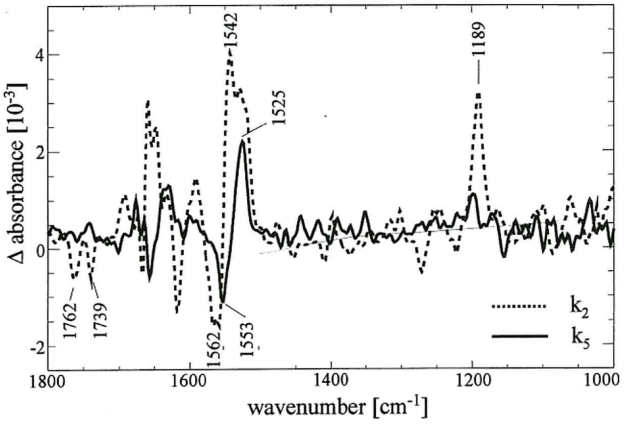

FIG. 9. The amplitude spectra of the rate constants $k_2 = 1.0 \cdot 10^4$ s^{-1} and $k_5 = 3.5 \cdot 10^4$ s^{-1} are shown, which describe the biphasic L-to-M transition.

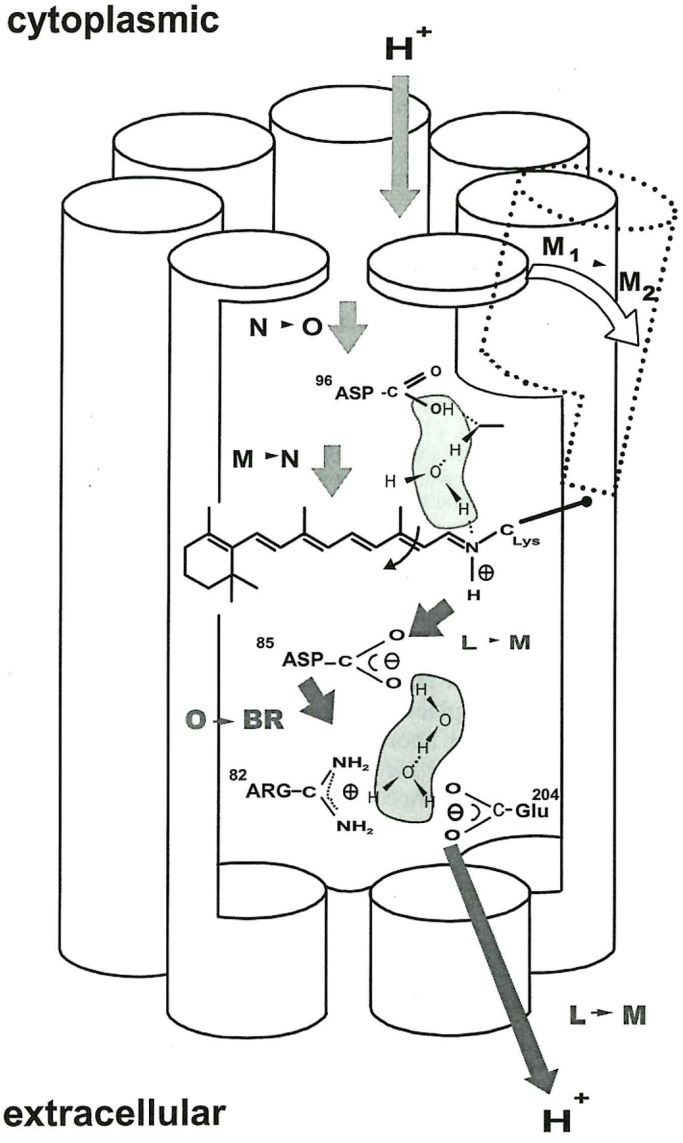

FIG. 10. The current model of the proton pump mechanism of bacteriorhodopsin, to which many groups have contributed (for references, see text). After the light-induced all-*trans* to 13-*cis* retinal isomerization in the BR-to-K transition, the Schiff base proton is transfered to Asp85 in the L-to-M transition. Simultaneously a proton is released from an ice-like H-bonded network to the extracellular site. This network is controlled by Glu204 and Arg82. Asp85 reprotonates the network in the O-to-BR reaction. The Schiff base is oriented in the M_1-to-M_2 transition from the proton release site to the proton uptake site by a small backbone movement and determines thereby the vectoriality of proton transfer. A larger backbone movement is observed in the M-to-N transition as compared to the M_1-to-M_2 transition. Asp96 reprotonates the Schiff base in the M-to-N transition. Asp96 itself is reprotonated from the cytoplasmic site in the N-to-O transition. Proton transfer between Asp96 and the Schiff base takes place via a water-like H-bonded network.

ular proton transfer in the L-to-M reaction (see Fig. 10). The band at 1188 cm^{-1} indicates the deprotonation of the Schiff base; the band at 1762 cm^{-1} shows the protonation of Asp85; and the difference bands at 1739 cm^{-1}/1742 cm^{-1} show the environmental change of Asp96; the band shift from 1542 to 1562 cm^{-1} indicates the shift of the C=C retinal stretching vibration in the L-to-M transition. On the other hand, the k_5 amplitude spectrum is dominated by a shift of the band from 1525 to 1553 cm^{-1}. This observation mostly represents the spectral changes in the M_1-to-M_2 transition revealed by double-flash experiments.[29] Interestingly only the rate constant k_2, of all proton transfer rate constants, shows a large kinetic isotope effect, a factor of 6 instead of $\sqrt{2}$, in D_2O as compared with H_2O.[30] Therefore we propose an hydrogen-bonded network proton transfer for the proton-release pathway and the proton-uptake pathway.[30] For details of the proposed proton pump mechanism, see Fig. 10.

With the time-resolved step-scan FT-IR technique, a very powerful tool is established by which molecular reaction mechanisms of proteins can be studied, with ms time resolution at the atomic level.

ACKNOWLEDGMENTS

This work war supported by the Deutsche Forschungsgemeinschaft, SFB 394, Teilprojekt C2. We thank Dr. David Rumschitzki for his help with English style corrections.

1. K. Gerwert, Current Opinion Structural Biology **3,** 769 (1993).
2. N. Grigorieff, T. A. Ceska, K. H. Downing, J. M. Baldwin, and R. Henderson, J. Mol. Biol. **259,** 393 (1996).
3. M. S. Braiman and K. Rothschild, Ann. Rev. Biophys. Chem. **17,** 541 (1988).
4. K. Gerwert, Biochim. Biophys. Acta **1101,** 147 (1992).
5. F. Siebert, in *Biomolecular Spectroscopy,* Part A, R. J. H. Clark and R. E. Hester, Eds. (Wiley, Chichester, 1993), p. 1.
6. J. Deisenhofer and H. Michel, EMBO J. **8,** 2149 (1989).
7. B. Robert, E. Nabedryk, and M. Lutz, in *Time Resolved Spectroscopy,* R. J. H. Clark and R. E. Hester, Eds. (Wiley, New York, 1989), pp. x–x.
8. W. Mäntele, in *The Photosynthetic Reaction Center,* J. Deisenhofer and J. Norris, Eds. (Academic Press, New York, 1993), Vol. II, p. 239.
9. R. Brudler, H. J. M. de Groot, W. B. S. van Liemt, W. F. Steggerda, R. Esmeijer, P. Gast, A. J. Hoff, J. Lugtenburg, and K. Gerwert, EMBO J. **13,** 5523 (1994).
10. J. A. McGray and D. Trentham, Annu. Rev. Biophys. Biophys. Chem. **18,** 239 (1989).
11. A. Wittinghofer and E. F. Pai, Trends Biochem. Sci. **16,** 382 (1991).
12. K. Gerwert, V. Cepus, A. Scheidig, and R. S. Goody, in *Time Resolved Vibrational Spectroscopy,* A. Lau, F. Siebert, and W. Werncke, Eds. (Springer-Verlag, Berlin, 1994), p. 256.
13. A. Barth, W. Kreutz, and W. Mäntele, Biochim. Biophys. Acta **1057,** 115 (1991).
14. A. Troullier, K. Gerwert, and Y. Dupont, Biophy. J. **71,** 2970 (1996).
15. M. Lübben and K. Gerwert, FEBS Lett. **397,** 303 (1996).
16. M. S. Braiman, P. L. Ahl, and K. J. Rothschild, Proc. Natl. Acad. Sci. USA **84,** 5221 (1987).
17. K. Gerwert, Ber. Bunsenges. Phys. Chem. **92,** 978 (1988).
18. K. Gerwert, G. Souvignier, and B. Hess, Proc. Natl. Acad. Sci. USA, **87,** 9774 (1990).
19. M. S. Braiman, O. Bousche, and K. J. Rothschild, Proc. Natl. Acad. Sci. USA **88,** 2388 (1991).
20. G. Souvignier and K. Gerwert, Biophy. J. **63,** 1393 (1992).
21. W. Uhmann, A. Becker, C. Taran, and F. Siebert, Appl. Spectrosc. **45,** 390 (1991).
22. R. A. Palmer, J. L. Chao, R. M. Dittmar, V. G. Gregoriou, and S. E. Plunkett, Appl. Spectrosc. **47,** 1297 (1993).
23. D. Oesterhelt and W. Stoeckenius, Methods Enzymol. **31,** 667 (1974).
24. B. Heßling, G. Souvignier, and K. Gerwert, Biophy. J **65,** 1929 (1993).
25. J. le Coutre, J. Tittor, D. Oesterhelt, and K. Gerwert, Proc. Natl. Acad. Sci. USA **92,** 4962 (1995).
26. M. Engelhard, K. Gerwert, B. Hess, W. Kreutz, and F. Siebert, Biochemistry **24,** 400 (1985).
27. M. S. Braiman, T. Mogi, T. Marti, L. J. Stern, H. G. Khorana, and K. J. Rothschild, Biochemistry **27,** 8516 (1988).
28. K. Gerwert, B. Hess, J. Soppa, and D. Oesterhelt, Proc. Natl. Acad. Sci. USA **86,** 4943 (1989).
29. B. Heßling, R. Rammelsberg, and K. Gerwert, Biophys. J., paper submitted.
30. J. le Coutre and K. Gerwert, FEBS Lett. **398,** 333 (1996).